Chainlike Au– O Structures on Au (110)-(1× r) Surfaces Calculated from First Principles

ARTICLE *in* THE JOURNAL OF PHYSICAL CHEMISTRY C · APRIL 2009

Impact Factor: 4.77 · DOI: 10.1021/jp810581s

Chainlike Au−O Structures on Au(110)-(1 × *r*) Surfaces Calculated from First Principles

M. Landmann,* E. Rauls,* and W. G. Schmidt*

Lehrstuhl für Theoretische Physik, Universität Paderborn, 33095 Paderborn, Germany

Received: December 2, 2008; Revised Manuscript Received: January 28, 2009

We present density functional theory calculations of the adsorption of atomic oxygen on the Au(110) surface. The stability of oxygen adstructures on various (1 × *r*) reconstructed surfaces has been investigated, considering experimentally typical ultrahigh vacuum (UHV) conditions. Three Au−O chainlike structures have been identified to be especially stable under specific temperature and pressure conditions. These chain structures are clearly favored over oxygen conglomerates on the (1 × *r*) surfaces and represent the most stable form of chemisorbed atomic oxygen on Au(110) surfaces.

Introduction

The noble metal gold is considered as a material of persisting beauty and value. The fact that gold does not oxidize in air and the resulting small number of existing gold oxides shows the low affinity of oxygen and gold toward each other. Due to this chemical inertness, gold has been seen for a long time as an uninteresting material for catalytic processes. The interest in the catalytic properties of gold changed later on upon findings that nanometer-sized gold particle catalysts supported on various metal oxides can be highly active in the field of carbon monoxide (CO) oxidation, even for temperatures as low as 70 K.[1−3]

The investigation of such catalytic reactions leads to the questions, how is the oxygen molecule activated and what is the nature of the involved Au−O preliminary stages and/or intermediates in these reactions? Especially the second part of this problem is directly related to the subject of this paper. In contrast to the investigation of free and supported nanoparticles/nanoclusters,[4−10] only a few theoretical and experimental studies were devoted to Au single crystal surfaces. With regard to CO oxidation, Gottfried et al. investigated adsorption of O and O_2[11−14] oxygen-precovered Au(110)-(1 × 2) surfaces.[15] While molecular oxygen chemisorption has been observed in the presence of surface impurities,[16,17] no dissociative O_2 chemisorption on clean, extended gold single crystal surfaces has been observed in recent studies. Sault et al.[18] studied O_2 adsorption on the missing row reconstructed Au(110) surface using O_2 pressures up to 1400 Torr and temperatures between 300 and 500 K. Under no circumstances was any dissociative adsorption of O_2 observed by thermal desorption spectroscopy (TDS). This has been confirmed by Gottfried et al.,[11] who pointed out that no desorption of O_2 is observed in TDS above 60 K after adsorption of oxygen on the surface under UHV conditions at a sample temperature of 28 K. This excludes a partial spontaneous conversion of physisorbed oxygen into chemisorbed oxygen.

To overcome the activation barrier to produce chemisorbed oxygen, different methods have been reported so far: thermal dissociation,[18,19] oxygen ion sputtering,[12] microwave discharge,[20] and the use of reactive molecules like NO_2 or O_3.[21] In their investigations, Gottfried et al.[11,13,14] produced chemisorbed oxygen on Au(110)-(1 × 2) by electron bombardment of physisorbed O_2 layers of oxygen molecules. The oxygen species, produced in that way, has been characterized by a single TDS desorption peak above 500 K. For low coverages, a second-order desorption kinetics indicated chemisorbed oxygen atoms. The corresponding adsorption energy was determined as 140 ± 3 kJ/mol. Another adsorption state around 490 K for higher coverages has been attributed to the decomposition of an oxide species.

The Au(110) single crystal surface shows a characteristic missing row structure at room temperature. As established by diffraction techniques[22,23] and scanning tunneling microscopy,[24,25] every second close-packed atomic row in the topmost atomic layer is missing in this surface reconstruction. As a result, the periodicity in the [001] direction is doubled with respect to the structurally relaxed, unreconstructed bulk truncated surface configuration Au(110)-(1 × 1). Every surface trench, developing due to reconstruction, consists of two (111)-microfacets. The Au(110)-(1 × 2) surface is known to undergo two phase transitions; on the one hand an Ising transition at ≈650 K, in which the surface deconstructs, and on the other hand a three-dimensional roughening transition at ≈700 K,[26,27] coming along with destruction of two-dimensional surface arrangements.

Additionally, surface reconstructions with deeper trenches (missing atoms in the second layer) and (1 × 3) periodicity have been observed on clean surfaces[22,24] and shown to be stable up to 350 K.[22] Furthermore, the appearance of a (1 × 3) reconstruction has been observed to occur upon Cs[28] or Ca adsorption.[29] Deeper corrugations than for Au(110)-(1 × 3) have not yet been observed.[24] (1 × 3) steps on Au(110) can be stable up to temperatures as high as 500 K, as confirmed by high-temperature STM.[27]

A recently observed property of gold is its tendency to form freely suspended metallic chains (atomic nanowires) during the mechanically controlled "breaking" of atomic-scale gold contacts.[30] These chain structures consist of one Au atom in diameter and several Au atoms (4−8 Au atoms[30,31]) in length and hence form a "quasi-one-dimensional" system. In line with theoretical investigations,[32] the observed[33] Au−Au distance in the created gold chains is 2.5 ± 0.2 Å under cryogenic vacuum conditions. In experimental high-resolution transmission electron microscopy (TEM) studies at room temperatures, unusually long Au−Au bond lengths of ≈3.0 − 3.6 Å[34] have been observed. Also even longer Au−Au distances up to ≈4.0 Å[35] were reported.

* Corresponding authors. E-mail: landmann@phys.upb.de (M.L.), rauls@phys.upb.de (E.R.), W.G.Schmidt@upb.de (W.G.S.).

10.1021/jp810581s CCC: $40.75
Published on Web 03/12/2009

A possible explanation of these unusually long Au−Au distances and the contradictory results is the incorporation of light foreign atoms (H,[36] C,[37] O[32]) in this type of nanostructures that cannot be observed in TEM. Bahn et al.[32] demonstrated in a DFT study on adsorption-induced restructuring of gold nanochains that these long Au−Au bonds are in agreement with the oxygen-binding properties of Au chains. The oxygen incorporation leads to a new type of Au−O nanochain that binds oxygen "unexpectedly" strong. The chemisorption energy of oxygen atoms in the considered Au−O chain has been calculated to 1.5 eV per two oxygen atoms relative to the energy of the free molecule. Furthermore, the conductance of one quantum unit is the same for the Au−O chains as for a pure gold chain.

In search of the reconstruction driving force of the Au(110) missing row surface, the reconstruction tendencies of gold, as well as its 5d periodic table neighbors, iridium (Ir) and platinum (Pt), have been related to strong relativistic effects in these elements.[38] Furthermore, it has been argued that the relativistic nature of gold[39,40] might represent the common origin of surface reconstruction and the formation of Au chainlike structures.[41,42] This argument is supported by the fact that suspended single-atom chains of silver (Ag), where the (110) surface does not show the reconstruction characteristics known from the Au(110) surface, are of two, or rarely three, single-atom lengths.[31] Recently, some studies demonstrated that oxygen not only stabilizes the formation of Au nanochains but also significantly enhances the formation of Ag chains.[31,42]

In this work, we extend our earlier investigations of the adsorption of atomic oxygen on various reconstructions of the Au(110) surface[43] to more complex oxygen adstructures and identify possibly stable oxygen adstructures by combining DFT total energy calculations with thermodynamics.[44−47]

The paper is organized as follows: In section II, we describe our methodological approach. In section III, the results of our calculations are presented and discussed, starting with a short description of the surfaces considered and then turning to a description of the geometries and energetics of various O/Au(110)-(1 × r) structures. The largest part of this section is dedicated to the description of chainlike Au−O structures on the surfaces and their thermodynamical stability. Our theoretical results are compared to experimental findings, and several sources for discrepancies in the stability range are discussed in detail. Finally, section IV summarizes the work.

Methodology

We have performed first principles density functional theory (DFT) calculations with the Vienna ab initio simulation package (VASP).[48] The Kohn−Sham equations were solved using the generalized-gradient XC-functional approximation proposed by Perdew and Wang (GGA-PW91).[49] The electron−ion interaction was described by the projector-augmented wave (PAW) method.[50,51] In the PAW data, scalar relativistic corrections are contained. Throughout this work, an energy cutoff of 400 eV was used to expand the wave functions into the plane wave basis sets. The Brillouin zone integration was performed using a cell size dependent Monkhorst−Pack *k*-point sampling.[52] Calculations in (2 × 2) surface unit cells (SUC) are based on (8 × 6 × 1) *k*-points. The *k*-point sets were chosen to have approximately the same *k*-point density for calculations using different sized SUCs. The first-order Methfessel−Paxton smearing method with a width of 0.2 eV has been used. For gas phase calculations of atomic and molecular oxygen, only the Γ-point has been used.

The surface slabs were modeled with eight layers of metal atoms and a vacuum region of ∼11.8Å. The two bottom layers of the surface slabs were frozen in bulk-truncated positions during the geometry relaxations. The positions of the gold atoms in the top six atomic layers as well as the positions of the O atoms placed on the upper site of the slab were optimized without any constraint, until forces on the atoms were less than 0.01 eV/Å. The dipole moment induced by the asymmetric slab geometry with different top and bottom side surfaces was taken into account by applying a dipole correction in the *z* direction. The methodology and numerical parameters of the present calculations have already been used in a foregoing study[43] and are very similar to related studies.[53−56] All unit-cell sizes are given as an integer multiple (*n* × *m*), *n*, *m* = 1, 2,... of the smallest surface unit cell of the Au(110)-(1 × 1) surface (cf. Figure 1).

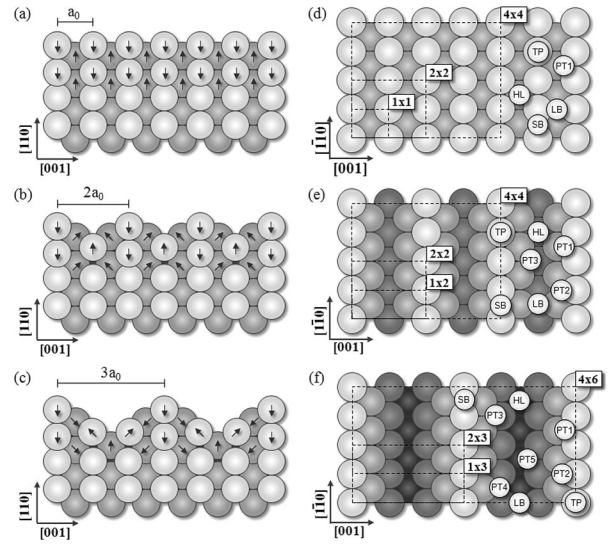

Figure 1. Schematic side views of the geometric shape of (a) the unreconstructed Au(110)-(1 × 1) and the reconstructed missing row type surfaces (b) Au(110)-(1 × 2) and (c) Au(110)-(1 × 3). Various considered adsorption sites (TP, top; SB, short bridge; LB, long bridge; HL, hollow; PT, pseudo-3-fold), as well as surface unit cells, are defined in the schematic top views of the (d) Au(110)-(1 × 1), (e) the Au(110)-(1 × 2), and (f) the Au(110)-(1 × 3) surfaces. Darker gray colored circles indicate gold atoms in deeper atomic layers, as seen from the respective point of view. The arrows indicate atom displacements in the optimized surface structures with respect to atom positions in truncated bulk configuration.

Adsorption energies are defined as an average over all oxygen atoms in the considered surface unit cell.

$$E_{ad} = -\frac{1}{N_O}(E_{sub,ad} - E_{sub} - N_O E_O) - \frac{1}{2}E_{b,O_2} \qquad (1)$$

Herein, $E_{sub,ad} = E_{sub,ad}(N_{Au}, N_O)$ is the total energy of the whole system containing N_{Au} gold atoms and N_O oxygen atoms. $E_{sub} = E_{sub}(N_{Au}, 0)$ is the total energy of the relaxed substrate containing the same number of gold atoms and E_O is the total energy of a free oxygen atom. By subtracting half the binding energy E_{b,O_2} of the gas phase oxygen molecule, the adsorption energy is given relative to molecular oxygen. Adsorption energies in terms of the foregoing definition describe a stable/exothermic adsorption process in the case of a positive sign and an unstable/endothermic process in the case of a negative sign.

To relate calculated structures to specific, experimentally relevant conditions, the temperature and pressure dependences of a surrounding molecular oxygen atmosphere have to be

considered. In this case, the equilibrium state of the surface is determined by minimization of the surface excess free energy[57] (per unit area) $\gamma = \Omega_S/A$. A represents the surface area of the relevant SUC.

$$\Omega_S = F_S - \sum_i \mu_i N_{iS} \tag{2}$$

where $\Omega_S = \Omega_S(T, A, \mu_i)$ is the surface excess contribution to the grand potential depending on T, A, and the chemical potentials μ_i of the involved atomic species. $F_S = F_S(T, A, N_{iS})$ is the surface excess free energy depending on the numbers N_{iS} of the various atomic species in the surface region. For simplicity, we will drop the index S and the "add-on" "surface excess" in the further discussion.

To determine the (most) stable oxygen adstructures with respect to the particular (clean) surface of interest, we evaluate the free energy of adsorption (per surface area) $\Delta\gamma_{ad}$.

$$\Delta\gamma_{ad} = -\frac{1}{A}(F_{sub,ad} - F_{sub} - N_O\mu_O - \Delta N_{Au}\mu_{Au}) \tag{3}$$

$F_{sub,ad} = F_{sub,ad}(T, A, N_{Au}, N_O)$ is the free energy of the total substrate−adsorbate system, $F_{sub} = F_{sub}(T, A, N_{Au}, 0)$ is the free energy of the substrate system, and $\mu_O = \mu_O(T, p_{O_2})$ and μ_{Au} are the chemical potentials of oxygen and gold. ΔN_{Au} denotes the difference in surface gold atoms, in the case of different surface reconstructions. If not stated otherwise, $F_{sub,ad}$ and F_{sub} are approximated by their leading terms, the DFT total energies $E_{sub,ad}$ and E_{sub}. Additionally, we considered the temperature dependence of the surface-slab total energies by calculating the vibrational entropy contributions TS_{vib} to the free energies $F_{sub,ad/sub} \approx E_{sub,ad/sub} - TS^{vib}_{sub,ad/sub}$. The entropy S_{vib} can be calculated on the basis of statistical physics (following refs 58, 59) via

$$S_{vib}(T) = k_B \sum_i \frac{h\nu_i}{k_BT}\frac{1}{\exp(h\nu_i/k_BT) - 1} - \ln[1 - \exp(-h\nu_i/k_BT)] \tag{4}$$

The sum runs over all vibrational frequencies ν_i of the particular system. These modes are obtained from the eigenvalues of the dynamical matrix containing the second derivatives of the energy with respect to the atomic positions. The dynamical matrix is constructed using central differences from the forces on each atom by displacing all nonfixed atoms in the three Cartesian directions. The atoms in the four/five bottommost atomic layers of the eight-layer (4 × 2)/(4 × 3) SUCs were kept fixed in frequency calculations for the (1 × 2)/(1 × 3)-surface systems.

The chemical potential of gold in eq 3 is identified by the energy E^{bulk}_{Au} of an Au atom in its bulk environment. The chemical potential of O atoms can be split into a (T, p_{O_2})-independent part, the total energy of a free O_2 molecule [$^1/_2E_{O_2} = {}^1/_2(E_O + E_{b,O_2})$], a (T, p_{O_2})-dependent part [$\Delta\mu_O(T, p_{O_2})$], and a neglected zero point energy term

$$\mu_O(T, p_{O_2}) \approx \frac{1}{2}E_{O_2} + \Delta\mu_O(T, p_{O_2}) \tag{5}$$

Hence, the free energies of adsorption are calculated via

$$\begin{aligned}\Delta\gamma_{ad} &\approx -\frac{1}{A}(F_{sub,ad} - F_{sub} - N_O\mu_O - \Delta N_{Au}E^{bulk}_{Au}) \\ &= \frac{N_O}{A}E_{ad} + \frac{T\Delta S_{vib}}{A} + \frac{N_O}{A}\Delta\mu_O + \frac{\Delta N_{Au}}{A}E^{bulk}_{Au} \\ &\approx \frac{N_O}{A}E_{ad} + \frac{N_O}{A}\Delta\mu_O + \frac{\Delta N_{Au}}{A}E^{bulk}_{Au}\end{aligned} \tag{6}$$

In the case of neglected vibrational entropy contributions, $\Delta S_{vib} = S^{vib}_{sub,ad} - S^{vib}_{sub}$, the whole temperature, pressure dependence is solely included in $\Delta\mu_O(T, p_{O_2})$. The chemical potential $\mu_O(T, p_{O_2})$ can be calculated using the partition function Z_{O_2} of a homonuclear diatomic molecular gas,[60,61] consisting of N dimers, via

$$\mu_O(T, p_{O_2}) = \frac{1}{2N}(-k_BT \ln Z_{O_2} + pV) \tag{7}$$

resulting in the temperature- and pressure-dependent term $\Delta\mu_O = -{}^1/_2k_BT\{\ln[(2\pi m_{O_2}h^{-2})^{3/2}(k_BT)^{5/2}p_{O_2}{}^{-1}]\} - {}^1/_2k_BT\{\ln[{}^1/_2k_BTB_r{}^{-1}] - \ln[1 - \exp(h\omega_0(k_BT)^{-1})]\} - 1/2k_BT(\ln g)$. B_r is the rotational constant of the O_2 molecule, ω_0 the vibrational frequency, and g the electronic ground-state spin degeneracy (cf. section 3.1 for reference values). Similar studies have been done before.[62,63]

Per definition, the most positive free energy of adsorption $\Delta\gamma_{ad}$ for a specific (T, p_{O_2}) condition identifies a stable O/Au(110) structure. As apparent from eq 6, the temperature and pressure influence scales with the ratio N_O/A that represents the oxygen concentration on the surface. There are two limiting cases for the stability of O/Au(110)-(1 × r) structures. On the one hand, according to results published before,[43] the clean Au(110)-(1 × 3) surface is the most stable surface, if entropic energy contributions are neglected,[64] for a low oxygen chemical potential, i.e., by a low oxygen concentration in the atmosphere. On the other hand, increasing the oxygen concentration, and thus the chemical potential, results in a bulk oxide. The first case is illustrated by a horizontal line in the $\Delta\gamma_{ad}$ versus $\Delta\mu_O(T, p)$ plots, the second case by a vertical line, i.e., an infinitely thick bulk oxide. A reasonable choice of $\Delta\mu_O(T, p_{O_2})$ for the transition to a bulk oxide structure consists of the heat of formation $H_f^{Au_xO_y}$ of the most stable gold oxide, Au_2O_3. Between both these border cases, one or more oxygen adstructures on the Au(110)-(1 × r) surfaces might be thermodynamically stable.

To analyze the O/Au(110)-(1 × r) systems, we calculated the induced charge densities

$$\Delta n(\mathbf{r}) = n_{tot}(\mathbf{r}) - n_{ad}(\mathbf{r}) - n_{sub}(\mathbf{r}) \tag{8}$$

They indicate regions of electron accumulation and depletion. Therein n_{tot} is the total electron density of the structurally relaxed total adsorbate−substrate system and n_{ad}/n_{sub} the electron densities of the adsorbate/substrate subsystem in the same position as in the total adsorbate−substrate system.

Results and Discussion

Reference Values. Within GGA-PW91 we calculated an equilibrium the unit of the lattice constant a_0 are Å = 4.176, a bulk modulus B_0 = 127 GPa, and a cohesive energy per Au atom of 3.17 eV. Considering the experimental values a_0 =

4.078,[65] B_0 = 172 GPa,[65] and a cohesive energy per gold of 3.81 eV,[66] this confirms the typical finding that GGA tends to underestimate chemical bond strengths.

The calculated O_2 molecule bond length is r_0 = 1.24 Å, the corresponding vibrational frequency ω_0 = 1556 cm^{-1} (≙193 meV), and the binding energy per oxygen atom is $^1/_2E_{b,O_2}$ = 3.08 eV (calculated spin polarized). Reported experimental values are ω_0 = 1580 cm^{-1} (≙196 meV), r_0 = 1.2074 Å[67] and $^1/_2E_{b,O_2}$ = 2.56 eV.[67]The rotational constant B_r is 1.445 cm^{-1} (≙0.179 meV)[68] and the O_2-ground-state spin degeneracy g = 3.

The heat of Au_2O_3 formation, per stoichiometric unit, has recently been calculated by Shi et al.[69] to be weakly exothermic: $H_f^{Au_2O_3}$ = −519 meV (−36 meV in an experiment[70] at 298.15 K). This value (−173 meV per O atom) has been chosen as the limit for the stability of the bulk oxide in the further discussion.

Surfaces. We investigated the interaction of atomic oxygen with three different Au(110) surfaces. These are the unreconstructed, structurally relaxed (1 × 1) surface and the two missing row type surfaces (1 × 2) and (1 × 3), characterized by doubled and tripled surface periodicity in the [001] direction. "Missing row" reconstructions stands for the removal of close-packed atomic rows from the topmost surface layers. In the case of the "common" missing row reconstruction, every second close-packed atomic row in the [1$\bar{1}$0] direction is missing, resulting in trenches, bordered by two (111)-microfacets. Higher order missing row reconstructions with (1 × r) periodicity can be generated by removing of (r − n) close-packed rows from the nth atomic layer [n = 1, 2,..., (r − 1)]. The structure of these surfaces is schematically illustrated in Figure 1. A detailed theoretical description of the structure of these surfaces, in the form of various characteristic parameters, and a discussion of surface energies can be found in ref 43.

Oxygen Adsorption. In our preceding investigation[43] of oxygen chemisorption, we investigated various $p(m \times n)$ atomic oxygen adlayers on (1 × r) surfaces. The considered adsorption sites pseudo-3-fold (PT), short bridge (SB), long bridge (LB), top (TP), and hollow (HL) are schematically illustrated in Figure 1d−f.

We had found that only adsorption in PT and SB sites results in stable structures. However, only the PT1 sites, located along the topmost close-packed atomic rows, show adsorption energies of significant magnitude, especially if almost every second PT1 site along the same side of the close-packed atomic rows is occupied. With this paper we extend our studies of chemisorbed oxygen to more complex adstructures, generated by systematic variations of on-surface oxygen coverages. The coadsorption of subsurface oxygen atoms is partially included. Since PT1 sites are the most stable ones, their occupation is the basis for nearly all considered O/Au(110)-(1 × r) systems that are schematically summarized in Figures 2, 3, and 4 for r = 1, 2, 3, respectively. The corresponding adsorption energies are listed in Table 1. The adsorption energies for p(n × m) oxygen adlayers in PT1 sites are summarized in Table 2. (cf. ref 43). From the adsorption energies in Table 1, it is immediately clear that the energetically most favorable structures contain only oxygen atoms in PT1 sites. These structures, composed by occupation of every or every second PT1 site on both sides along the close-packed atomic rows, possess strong chain characteristics, as we will demonstrate in the following section. Therefore, we will refer to a surface structures like X1, Y1, and Z1 (cf. Figures 2−4) as symmetric Au−O chain (SC) and to a surface structures like X2, X3, Y2, and Z2 as asymmetric chain (AC). The adsorption energy differences between SC (Y1, Z1) and AC (X2, Z2) structures on the reconstructed surfaces are 42(±4) meV (cf. Table 1) and, thus, almost independent from the particular order r of (1 × r)-missing row reconstruction. Unlike to oxygen adsorption on reconstructed surfaces, the SC structure X1 (cf. Figure 2) is energetically less stable on Au(110)-(1 × 1). Furthermore, there are two different AC structures X2 and X3, in which every or every second topmost atomic row is involved in the chain formation. The adsorption energy for the X2 structure is slightly higher, due to the formation of a more ordered Au−O adlayer (cf. Figure 5) in contrast to X3.

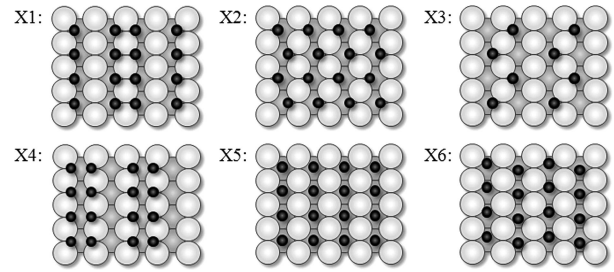

Figure 2. Schematic top views of the considered arrangements of oxygen atoms (black colored circles) on the Au(110)-(1 × 1) surface. Darker gray colored circles indicate gold atoms in deeper atomic layers.

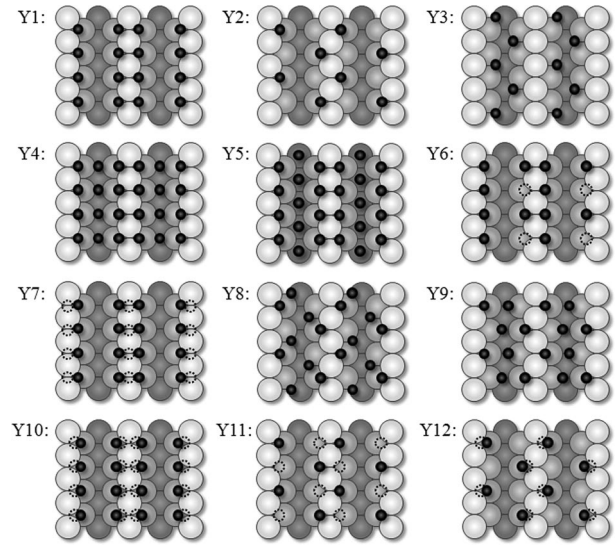

Figure 3. Schematic top views of the considered arrangements of oxygen atoms (black colored circles) on the (1 × 2) surface. Darker gray colored circles indicate gold atoms in deeper atomic layers. Dashed circles indicate the position of subsurface oxygen atoms located between the second and third layer of gold atoms.

As in the case of an isolated atom on the surface[71] (cf. Table 2), the adsorption energies for the chainlike structures are increased on the reconstructed surfaces but differ only marginal between different reconstructions (cf. Table 1).

Compared to oxygen adlayers of the p(n × m) type, the adsorption in the Au−O chain structures is more favorable on all investigated Au(110)-(1 × r) surface types. The coadsorption of oxygen atoms in non-PT1 sites significantly lowers the adsorption energy per oxygen atom. The same is true for coadsorption in subsurface sites (cf. Y6, Y7, Y10, Y11, Y12 in Table 1).

On the basis of these results, we will now discuss the structure and subsequent the energetics of the chainlike Au−O structures in more detail.

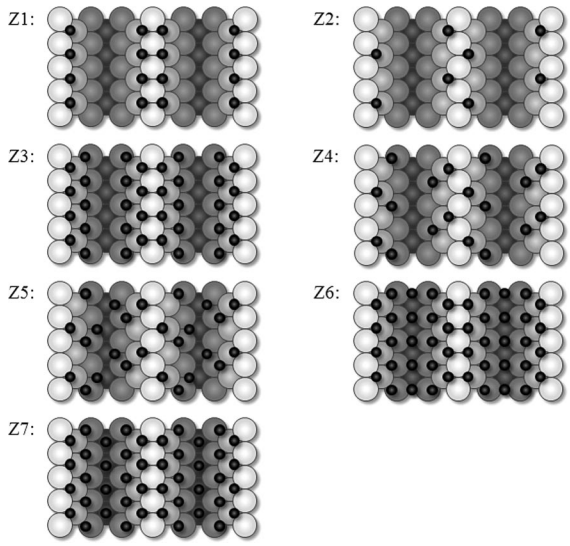

Figure 4. Schematic top views of the considered arrangements of oxygen atoms (black colored circles) on the Au(110)-(1 × 3) surface. Darker gray colored circles indicate gold atoms in deeper atomic layers.

TABLE 1: Adsorption Energies (E_{ad}, meV) Calculated via Eq 1 for All Investigated O/Au(110)-(1 × r) Structures Pictured in Figures 2−4[a]

adsorption energies (E_{ad}, meV)		
O/Au(110)-(1 × 1)	O/Au(110)-(1 × 2)	O/Au(110)-(1 × 3)
X1: 244	**Y1**: 393	**Z1**: 399
X2: 298	**Y2**: 439	**Z2**: 437
X3: −284	Y3: −222	Z3: −170
X4: −370	Y4: −129	Z4: 115
X5: −210	Y5: −67	Z5: 96
X6: −206	Y6: −9	Z6: −409
	Y7: −51	Z7: −389
	Y8: 14	
	Y9: −189	
	Y10: 63	
	Y11: −193	
	Y12: −419	

[a] The bold printed structure names refer to chainlike structures.

TABLE 2: Adsorption Energies (E_{ad}, meV) for Different Atomic Oxygen Coverages (Θ) of Au(110)-(1 × r) Surfaces in PT1 Sites[a]

surface	adlayer	Θ (Å^{-2})	E_{ad} (meV)
Au(110)-(1 × 1)	p(1 × 1)	0.081	−331
Au(110)-(1 × 1)	p(2 × 2)	0.041	**156**
Au(110)-(1 × 1)	p(4 × 4)	0.020	**172**
Au(110)-(1 × 2)	p(1 × 2)	0.041	−8
Au(110)-(1 × 2)	p(2 × 2)	0.020	**331**
Au(110)-(1 × 2)	p(4 × 4)	0.005	**328**
Au(110)-(1 × 3)	p(1 × 3)	0.027	−23
Au(110)-(1 × 3)	p(2 × 3)	0.014	**342**
Au(110)-(1 × 3)	p(4 × 6)	0.003	**349**

[a] Bold printed adsorption energies imply stable adsorption.

Au−O Chainlike Surface Structures. Figures 5−7 show detailed drawings of the Au−O chain structures on the different (1 × r) surfaces whose structural properties are described in this section.

At first sight it is apparent that all oxygen atoms involved in the formation of the chain structures retain their pseudo-3-fold coordinated form, which has been shown to be much more stable than all other adsorption sites.[43] The Au−O bond length of 2.03 Å in the Au−O chain is identical for the SC and the AC structure on both reconstructed surfaces. It differs only marginal (2.02 Å) for the two different ACs X2 and X3 on the unreconstructed (1 × 1) surface and is the same in the SC X1 on the (1 × 1) surface. In all SC structures (cf. Figure 5a−7a) the gold and oxygen atoms that are involved in the chain formation are arranged in a planar structure parallel to the surface plane with variations of ±0.03 toward the surface normal. In ACs the chain-gold atoms are placed slightly below the plane defined by the oxygen atoms. This displacement of gold atoms increases with stronger surface roughening. The smallest displacement of 0.07 Å is found in case of the AC X2,which is formed by an ordered Au−O adlayer (cf. Figure 5b). The bisection of the X2 oxygen coverage increases the displacement to 0.10 Å (cf. Figure 5c). For the (1 × 2) surface

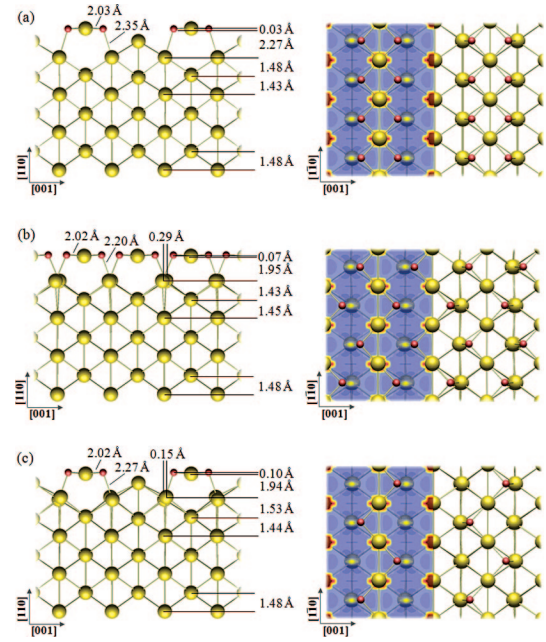

Figure 5. Detailed side and top views of the most favorable O/Au(110)-(1 × 1) surface structures: (a) the SC structure X1, (b) the AC structure X2, and (c) a the second AC structure X3. On the left, the structure of the geometrically relaxed structures is characterized by Au−O bond lengths and interplanar distances. The distance between the two lowest atomic layers represents the ideal bulk distance of 1.48 Å. On the right, the corresponding top views are shown. The PES for adsorption of atomic oxygen on Au(110)-(1 × 1) is partially shown (blue, high adsorption energy $E_{ad,O}$; red, low adsorption energy $E_{ad,O}$; a detailed description of the PESs is given in ref 43).

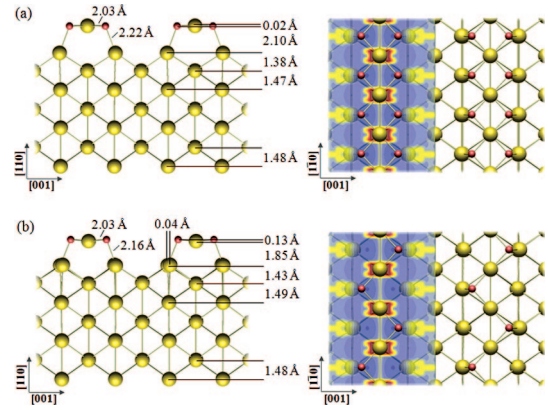

Figure 6. Detailed side and top views of the most favorable O/Au(110)-(1 × 2) surface structures: (a) the SC structure Y1 and (b) the AC structure Y2. (cf. Figure 5).

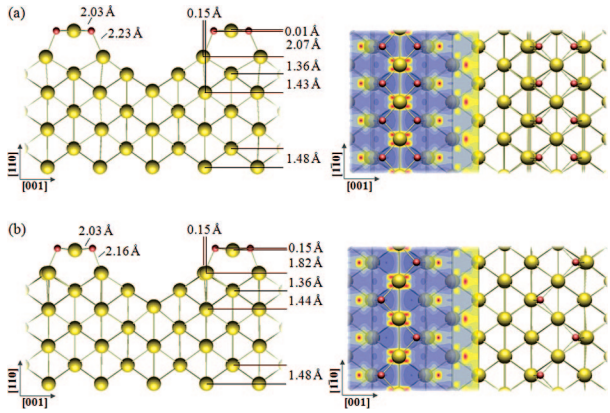

Figure 7. Detailed side and top views of the most favorable O/Au(110)-(1 × 3) surface structures: (a) the SC structure Z1 and (b) the AC structure Z2. (cf. Figure 5).

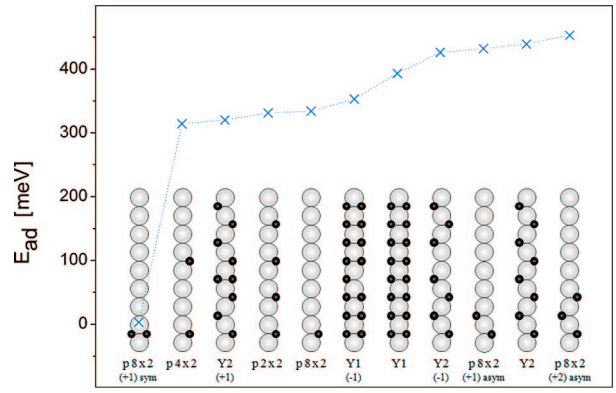

Figure 8. Adsorption energies E_{ad} (meV) for various PT1 coverages of the (1 × 2) surfaces (8 × 2) SUC. In the schematic drawings, the dark-colored circles represent oxygen atoms and light-colored circles Au atoms in the topmost layer. The numbers in the brackets indicate the number of added/removed oxygen atoms for the particular structure.

chain Y2 the chain-gold atoms are located 0.13 Å below the oxygen (cf. Figure 6b). In the AC structure Z2 on the (1 × 3) surface,this value reaches 0.15 Å (cf. Figure 7b). The Au−O bond between the oxygen atoms and the surface gold atoms is slightly increased compared to the Au−O bond lengths inside the chains. In the of the reconstructed surfaces, these bond lengths are 2.22/2.23 Å for the SC Y1/Z1 and 2.16 Å for the ACs Y2/Z2. In the case of the unreconstructed surface, they are a bit longer (2.35 Å for the SC X1; 2.20 and 2.27 Å for the ACs X2 and X3).

The formation of the Au−O chains due to oxygen adsorption generally increases the distance of the first layer atoms involved in the chain formation and the underlying second layer gold atoms (bulk interlayer spacing 1.48 Å). Especially the inward relaxation[43] of first layer gold atoms of the clean surfaces vanishes. For AC structures Y2 and Z2, the distance between chain and surface planes (defined by averaging over the particular Au/O positions) is 1.83 ± 0.02 Å. For the SCs Y1 and Z1 this distance is 2.08 ± 0.02 Å. In the case of the unreconstructed surface, these distances are somewhat larger (2.27 Å for X1 and 1.94 ± 0.01 Å for X2 and X3).

The structural similarity of SC and AC on various surface modifications allows unambiguously for the notation of these structures as a class of its own. Structures of this class are formed without exception by accumulation of the oxygen atoms along close-packed rows of gold atoms. These rows, especially characteristic for the missing row type reconstruction, represent a low coordinated form of gold atoms on extended surfaces. This suggests interpreting the formation of freely suspended, quasi-one-dimensional Au−O chains in which oxygen atoms enhance the chain formation[31,42] as a common general feature of the Au−O interaction.

Au−O Chain formation. In Figure 8, some adsorption energies are summarized from calculations using an (8 × 2) SUC. Starting with a single oxygen atom in the SUC, the adsorption energy $E_{ad,O}$ is 334 meV. The addition of one O atom is energetically most favorable (E_{ad} = 432 meV) in one of two diagonally obverse PT1 sites [i.e., forming the source of an AC structure (cf. p8 × 2(+1)asym)]. Adding a third O atom to this structure in an AC configuration results in an even higher adsorption energy of 453 meV [cf. p8 × 2(+2)asym]. For comparison, the adsorption of one additional O atom in the direct obverse PT1 site reduces the adsorption energy significantly to only 3 meV [cf. p8 × 2(+1)sym]. In general, all asymmetric oxygen arrangements allow favorable adsorption with E_{ad} > 420 meV. Therefore, the formation of any kind of well-ordered p(m × n) adlayer [cf. Table 2 for p(1 × 2), p(2 × 2), and p(4 × 4) and Figure 8 for p(4 × 2) and p(8 × 2)] that reaches adsorption energies <330 meV seems implausible. The coadsorption of O atoms on AC domains, i.e., the smattering formation of small SC domains [cf. Y2(+1)], is commonly connected to lower adsorption energies (<360 meV). Nevertheless, a complete SC structure is stabilized to E_{ad} = 393 meV. Accordingly, the adsorption energy for the last oxygen atom of the SC is very high (≈1000 meV). This stresses the special role of the SC structure.

As a result of the energetics presented above, one should expect the formation of small AC domains on the (1 × 2) surface in the case of very low oxygen concentrations. The formation of SC domains can first be expected after a maximal number of oxygen atoms arranged in asymmetric configurations. The following section deals with the question of how this behavior reflects itself in the thermodynamical stability of these chain structures under given atmospheric (T, p_{O_2}) conditions.

Temperature and Pressure Dependence. In Figure 9, the free energies of adsorption $\Delta\gamma_{ad}$ (without entropy contributions) versus the temperature- and pressure-dependent part of the chemical potential $\Delta\mu_O(T, p_{O_2})$ are plotted separately for each of the three surfaces. A stable structure is identified by the lowest $\Delta\gamma_{ad}$ line, i.e., the highest free energy of adsorption. The numbered areas indicate the stability of the particular clean surface (I), one or more possible stable oxygen adstructures or surface oxides (II), and the stable Au_2O_3 bulk oxide (III), whereas the oxide stability limit is given by the heat of formation of the particular oxide (cf. section 3.1). For clarity, only the O/Au(110)-(1 × r) structures with positive adsorption energy E_{ad} at T = 0 K and the most stable PT1 p(m × n) adlayer structure are shown.

Generally speaking, the investigated chain structures show common energy characteristics. For the two reconstructed surfaces, both the SC structures Y1 and Z1 and the AC structures Y2 and Z2 become stable for specific values of $\Delta\gamma_{ad}$. The ACs are stable for a lower (more negative) oxygen chemical potential. Qualitatively the SC X1 and AC X3 on the unreconstructed (1 × 1) surface show the same characteristics. Due to the different surface morphology of the unreconstructed surface, the second asymmetric Au−O surface structure X2 becomes most stable by forming a highly ordered Au−O adlayer structure (cf. detailed adlayer structure in Figure 5b).

In Figure 10, the free energies of adsorption of the most stable O/Au(110)-(1 × r) structures are shown. The clean (1 × 2)

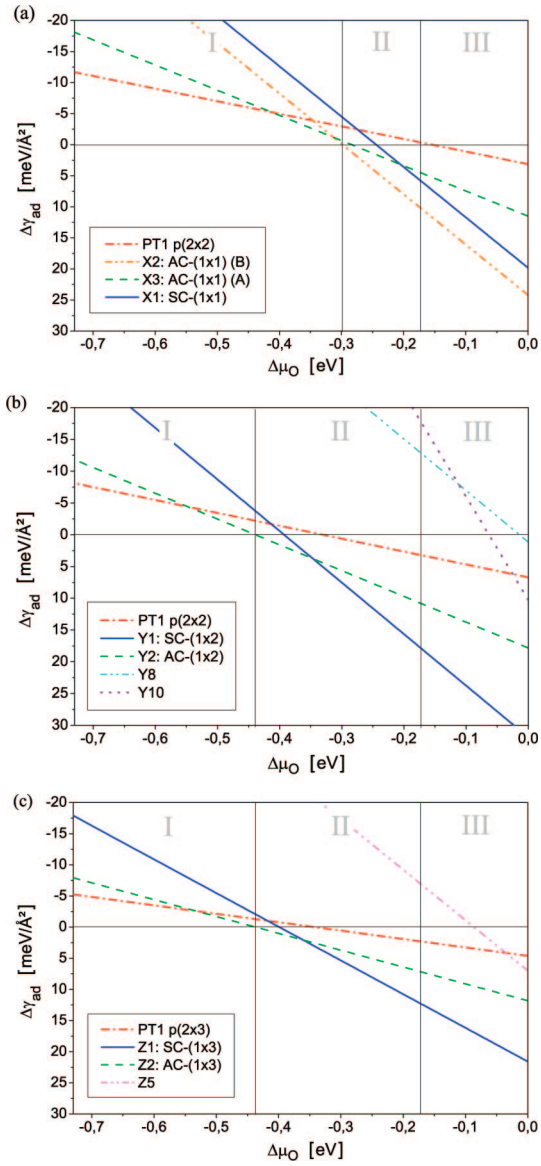

Figure 9. Free energy of adsorption (without entropy contributions) plotted versus $\Delta\mu_O(T, p_{O_2})$ for (a) the unreconstructed Au(110)-(1 × 1) surface and (b) the reconstructed Au(110)-(1 × 2) and (c) the Au(110)-(1 × 3) surfaces. A stable structure is identified by the lowest $\Delta\gamma_{ad}$ line (highest free energy of adsorption). The different numbered areas indicate the stability of (I) the clean (1 × *r*) reference surface, (II) possible stable structures containing on-surface oxygen, and (III) a stable bulk oxide.

surface was selected as reference surface (i.e., this structure is represented by the $\Delta\gamma_{ad} = 0$ line). To relate the results to atmospheric conditions, the temperature and pressure dependence of $\Delta\gamma_{ad}$ has been transferred to a temperature dependence at two specific constant O_2 pressures p_{O_2} (the two upper *x*-axis). The pressure $p_{O_2} = 1013$ mbar, associated with the topmost *x*-axis *T**, represents normal pressure. The second temperature axis *T* stands for $p_{O_2} = 5 \times 10^{-11}$ mbar and therefore for characteristic UHV conditions. Since the second case represents relevant experimental conditions given in ref 11, we limit the discussion to them.

Our calculations identify three stable oxygen adstructures that exclusively belong to the reconstructed surface type. The most stable O/Au(1 × 1) structure X2 is clearly the most unfavorable one in Figure 10. Therefore, we do not expect any O adstructure to become stable on the unreconstructed Au(110) surface. For

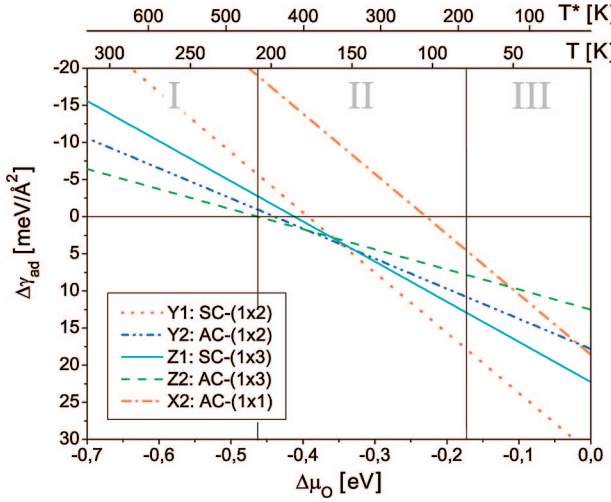

Figure 10. Free energy of adsorption (without entropy contributions) plotted versus $\Delta\mu_O(T, p_{O_2})$ in consideration of the various surface reconstructions with Au(110)-(1 × 2) as reference surface. The upper temperature axis *T** is given for constant pressure $p_{O_2} = 1013$ mbar. The second temperature axis *T* is for $p_{O_2} = 5 \times 10^{-11}$ mbar (UHV). A stable structure is identified by the lowest $\Delta\gamma_{ad}$ line (highest free energy of adsorption). The different numbered areas indicate the stability of (I) the clean (1 × 3) surface, (II) possible stable structures containing on-surface oxygen, and (III) a stable bulk oxide.

low oxygen coverages, the clean (1 × 3) surface is the most favorable structure. In Figure 10, this surface is almost identical to the *x*-axis, because of the very small difference in (1 × 2) and (1 × 3) surface energies (cf. ref 43) and therefore are not drawn explicitly. When the chemical potential is increased, the AC Z2 on the (1 × 3) surface represents the most stable structure for 178−210 K. Between 158 and 178 K, the AC Y2 is slightly more stable than the other chains. Finally, the SC Y1 (containing a maximal amount of on-surface oxygen in PT1 sites) is stable between 80 and 158 K, before the bulk oxide represents the most favorable structure with $\Delta\mu_O$ reaching the heat of formation of the Au_2O_3 oxide. Please note that also the SC structure on the (1 × 3) surface is very close in energy.

Apparently, the AC can be thermodynamically stable both on the (1 × 2) and on the (1 × 3) surface. There are two reasons for the change of the thermodynamic stability between the ACs independent of the chemical potential. First, oxygen adsorption on (1 × *r*) surfaces' PT1 sites ($r = 2$ or 3) is almost independent of the particular reconstruction.[43] Second, the order of reconstruction *r* defines the number of available PT1 sites. According to eq 6, which by the ratio N_O/A determines the slope of $\Delta\gamma_{ad}$, the O/Au(110)-(1 × 3) AC structure can be more stable than the Au(110)-(1 × 2) AC structure for very low values of the oxygen chemical potential. This is also in a more general context the reason for the ACs to become favored over the respective SC structures. They contain half (Y2) or less (Z2) of the amount of oxygen contained in the SC Y1, which is clearly favored over the ACs for an increasing chemical potential.

In contrast to experimental findings applying thermal desorption spectroscopy (TDS)[11] that show oxygen to desorb from the surface above 500 K, the applied theoretical methodology predicts desorption already above 210 K. In order to explain this discrepancy, further aspects have to be considered.

The first point is the unknown structure of the experimentally observed Au−O surface. Small oxide-like domains or an unconsidered subsurface adsorption might be able to explain the discrepancy. However, the coadsorption of subsurface oxygen atoms (cf. Y6, Y7, Y10, Y11, Y12) did not result in any favorable structure.

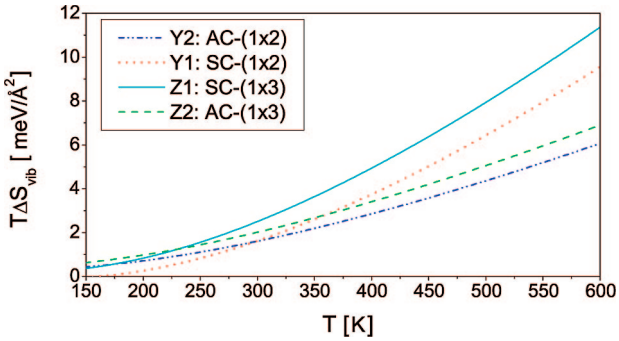

Figure 11. Calculated vibrational entropy contributions to the free energies of adsorption. Pictured are the entropic energy differences $T\Delta S_{vib} = T(S_{vib}^{sub,ad} - S_{vib}^{sub})$ between the total and the substrate system, multiplied with the temperature T.

Another source of error is the inclusion of the free energies only up to their leading terms. If the surface structures differ too strongly, the cancelation in the so far not included entropy terms is incomplete, and the common practice of neglecting these contributions is no longer justified. To clarify this point, we calculated the vibrational entropy contributions for the SCs Y1 and Z1, the ACs Y2 and Z2, and the clean substrate systems Au(110)-(1 × 2) and Au(110)-(1 × 3). The lattice vibrations of the two clean surfaces turned out to be very similar. They are characterized by a wide frequency band between 20 and 150 cm^{-1}. These frequency bands are only marginally changed if oxygen is adsorbed on the surfaces. In the high frequency region, in contrast, oxygen adsorption induces additional modes. The ACs show some single frequencies between 325 and 400 cm^{-1} and a frequency group from 450 to 575 cm^{-1}. The SCs show a few isolated frequencies in the range of 200−375 cm^{-1} and at 450 cm^{-1} and a group of modes between 500 and 575 cm^{-1}. For both the SCs and the ACs, the high-frequency modes belong to oxygen vibrations in the plane of the chain adstructure. The isolated modes distributed between 200 and 400 cm^{-1} are caused by oxygen movements perpendicular to the surface.

As explained in ref 43, the consideration of the vibrational entropy contributions leads to a stabilization of the clean (1 × 2) surface over the clean (1 × 3) surface at room temperature.

In Figure 11, the $T\Delta S_{vib}$ contributions are shown for the temperature range 150−600 K. ΔS_{vib} has been calculated as the difference between the entropy of the system with adstructure and that of the clean surface. Below 150 K, these contribution are negligible. Qualitatively, the SC and the AC contributions show the same temperature dependence, but the energy curves for the (1 × 3) surface are nearly constantly shifted to higher energies compared to the (1 × 2) curves. These entropic energies add to the $\Delta\gamma_{ad}$ values in Figure 10 and therefore modify the stability range of the adsorbate structures as shown in Figure 12. Thereby, the stability range of the AC Z2 is increased from 178−210 to 176−235 K. For the AC Y2 and the SC Y1, the stability range remains nearly unchanged.

A third reason for the discrepancies between theory and experiment is given by the failure of calculated DFT binding energies of the oxygen molecule. The experimental value for half the binding energy $^1/_2E_{b,O_2}$ is 2.56 eV. The GGA significantly overestimates this value as known from other studies:[72,73] $^1/_2E_{b,O_2}^{GGA} = 3.08$ eV. This value for the binding energy has been used to calculate the free energies of adsorption (cf. eq 6). In contrast to the free energy differences ($F_{sub,ad} - F_{sub}$) that enter the free energies of adsorption, this DFT error is not partially canceled out. We repeated, therefore, the calculations of the $\Delta\gamma_{ad}$ curves in Figure 10 using the experimental value. The use

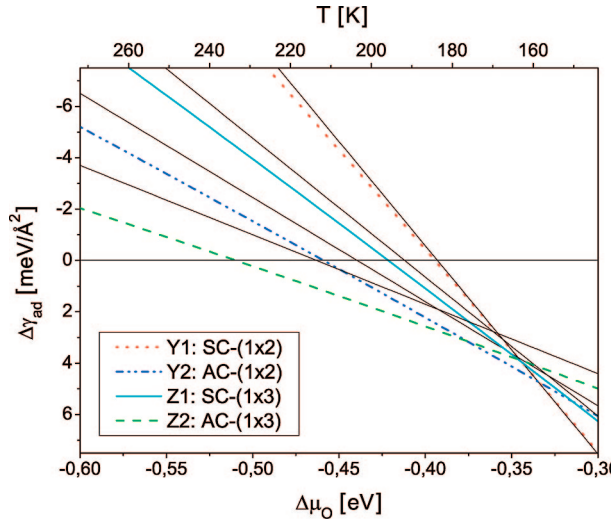

Figure 12. Free energies of adsorption including the vibrational entropy contributions ΔS_{vib} (cf. Figure 11). The plotted black lines reflect the situation in Figure 10. The upper (temperature) x-axis is given for constant pressure $p_{O_2} = 5 \times 10^{-11}$ mbar (UHV).

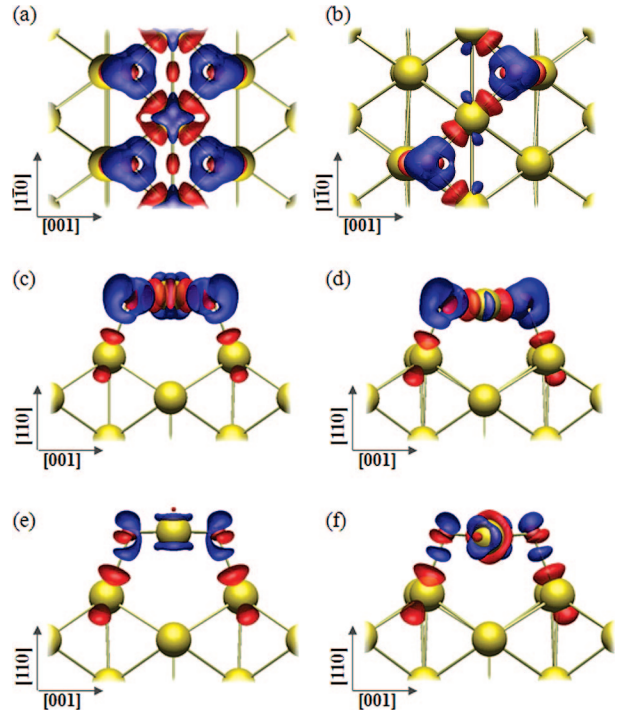

Figure 13. Charge-density differences (isosurface values ±0.055 e/Å^3) induced by oxygen adsorption in SC Y1 (a, c) and in AC Y2 (b, d) on the (1 × 2) surface and charge-density differences induced by adsorption of the whole SC (e) and AC (f). Blue indicates regions of electron accumulation and red regions of electron depletion.

of the experimental binding energy results in an enormous shift of the $\Delta\gamma_{ad}$ lines to higher temperatures. In detail, the stability ranges are now 403−438 K for Z2, 403−384 K for Y2 and 80−384 K for Y1 for an oxygen pressure of $p_{O_2} = 5 \times 10^{-11}$ mbar.

Summarizing, we can conclude that our calculations qualitatively confirm the experimental findings. Quantitatively, these sources of error discussed above correct the results into the right direction: the consideration of vibrational energy contributions and especially the failure of GGA O_2-binding energies reduce the theory−experiment gap.

Adsorption-Induced Charge Densities. As an example of the charge redistribution due to adsorption of atomic oxygen on Au(110) monocrystal surfaces, the regions of electron accumulation and depletion for the (1 × 2) surface's SC and AC are displayed in Figure 13. The charge density differences (CDD) pictured in Figure 13a−d demonstrate the charge density modification due to the oxygen interaction with the surface. As demonstrated before for "single" O atoms,[43] the bonding between O atoms and Au-surface/Au-chain atoms involves mainly the depletion of 5d-like Au orbitals pointing in direction of the Au−O bonds and a charge transfer into the O orbitals pointing toward the vacuum region.

In addition, the CDD between the total system and the chain structure as a whole and the substrate system are pictured in Figure 13e,f. These confirm that the chain structure is only bonded to the surface by Au−O bonds. Both in the SC and in the AC the Au−Au bonds between first layer Au atoms (now chain Au atoms) and second layer atoms (now topmost layer atoms of the remaining Au surface) vanish. The Au atoms in the chain structure are only linearly 2-fold coordinated to each other. The main influence of the chain structure on the charge density of the Au surface is limited to the directly bonded surface Au atoms. Consequently, the substrate is only slightly modified.

Summary

In summary, we have shown that chainlike Au−O structures represent the most stable form of atomic oxygen, chemisorbed on extended Au(110) surfaces. Likewise, in our foregoing study, which mainly focused on the adsorption of "single" oxygen atoms on the surface, the oxygen adsorption in chainlike structures is stronger in the case of missing row type reconstructed surfaces. We found two different chain configurations on each Au(110) surface to be the most stable oxygen adstructures. These symmetric and asymmetric Au−O chain structures differ by a factor of 2 in the amount of oxygen contained on the surface. Our results, based on atomistic thermodynamics, show that both of these structures are thermodynamically stable on the (1 × 2) reconstructed Au(110) surface. Also the asymmetric chain on the (1 × 3) surface becomes stable at a low oxygen chemical potential due to the larger separation of the close-packed atomic rows in the topmost layer. Alternative arrangements of atomic oxygen on the surface are clearly ruled out by comparison to these chain structures.

Our results strongly suggest that chainlike Au−O structures will form on Au(110) surfaces, when they are in contact with low concentrations of atomic oxygen. Therefore, they provide an interesting starting point for further investigations on the catalytic properties of (reconstructed) Au-monocrystal surfaces and the beginning of the oxidation process of these surfaces.

Our investigations mainly focused on adsorption on the various surfaces. Future discussions should deal with the question of how higher oxygen concentrations result in the formation of complex multilayer oxide structures. Experimentally,[11] these oxide structures have been assigned to the complicated structure of Au_2O_3.

Finally, our results directly connect the well-known missing-row surface reconstruction of the Au(110) surface with the formation tendency of pure and oxygen-supported suspended Au nanochains that have been reported in the recent past.

Acknowledgment. We appreciate support by the Deutsche Forschungsgemeinschaft (DFG) and the Höchstleistungsrechenzentrum Stuttgart (HLRS).

References and Notes

(1) Haruta, M.; Kobayashi, T.; Sano, H.; Yamada, N. *Chem. Lett.* **1987**, 405–408.
(2) Haruta, M.; Tsubota, S.; Kobayashi, T.; Kageyama, H.; Genet, M. J.; Delmon, B. *J. Catal.* **1993**, *144*, 175–192.
(3) Kim, T. S.; Stiehl, J. D.; Reeves, C. T.; Meyer, R. J.; Mullins, C. B. *J. Am. Chem. Soc.* **2003**, *125*, 2018–2019.
(4) Valden, M.; Lai, X.; Goodman, D. W. *Science* **1998**, *281*, 1647–1650.
(5) Mills, G.; Gordon, M. S.; Metiu, H. *J Chem. Phys.* **2003**, *118*, 4198–4205.
(6) Franceschetti, A.; Pennycook, S. J.; Pantelides, S. T. *Chem. Phys. Lett.* **2003**, *374*, 471–475.
(7) Molina, L. M.; Hammer, B. *Phys. Rev. B* **2004**, *69*, 155424.
(8) Molina, L. M.; Rasmussen, M. D.; Hammer, B. *J. Chem. Phys.* **2004**, *120*, 7673–7680.
(9) Molina, L.; Hammer, B. *Appl. Catal. A* **2005**, *291*, 21–31 (catalysis by gold).
(10) Kimble, M. L.; Castleman, A. W.; Mitric, R.; Burgel, C.; Bonačic-Koutecky, V. *J. Am. Chem. Soc.* **2004**, *126*, 2526–2535.
(11) Gottfried, J. M.; Schmidt, K. J.; Schroeder, S. L. M.; Christmann, K. *Surf. Sci.* **2002**, *511*, 65–82.
(12) Gottfried, J. M.; Elghobashi, N.; Schroeder, S. L. M.; Christmann, K. *Surf. Sci.* **2003**, *523*, 89–102.
(13) Gottfried, J. M.; Schmidt, K. J.; Schroeder, S. L. M.; Christmann, K. *Surf. Sci.* **2003**, *525*, 184–196.
(14) Gottfried, J. M.; Schmidt, K. J.; Schroeder, S. L. M.; Christmann, K. *Surf. Sci.* **2003**, *525*, 197–206.
(15) Gottfried, J. M.; Christmann, K. *Surf. Sci.* **2004**, *566−568*, 1112–1117 (Proceedings of the 22nd European Conference on Surface Science).
(16) Schrader, M. E. *Surf. Sci.* **1978**, *78*, L227–L232.
(17) Pireaux, J.; Chtaïb, M.; Delrue, J.; Thiry, P.; Liehr, M.; Caudano, R. *Surf. Sci.* **1984**, *141*, 211–220.
(18) Sault, A. G.; Madix, R. J.; Campbell, C. T. *Surf. Sci.* **1986**, *169*, 347–356.
(19) Canning, N.; Outka, D.; Madix, R. *Surf. Sci.* **1984**, *141*, 240–254.
(20) Linsmeier, C.; Wanner, J. *Surf. Sci.* **2000**, *454−456*, 305–309.
(21) Parker, D. H.; Koel, B. E. *J. Vac. Sci. Technol. A* **1990**, *8*, 2585–2590.
(22) Moritz, W.; Wolf, D. *Surf. Sci.* **1979**, *88*, L29–L34.
(23) Moritz, W.; Wolf, D. *Surf. Sci.* **1985**, *163*, L655–L665.
(24) Binnig, G.; Rohrer, H.; Gerber, C.; Weibel, E. *Surf. Sci.* **1983**, *131*, L379–L384.
(25) Gritsch, T.; Coulman, D.; Behm, R.; Ertl, G. *Surf. Sci.* **1991**, *257*, 297–306.
(26) Sturmat, M.; Koch, R.; Rieder, K. H. *Phys. Rev. Lett.* **1996**, *77*, 5071–5074.
(27) Koch, R.; Sturmat, M.; Schulz, J. J. *Surf. Sci.* **2000**, *454−456*, 543–551.
(28) Häberle, P.; Fenter, P.; Gustafsson, T. *Phys. Rev. B* **1989**, *39*, 5810–5818.
(29) Michaelis, R.; Kolb, D. *Surf. Sci.* **1990**, *234*, L281–L284.
(30) Yanson, A. I.; Rubio Bollinger, G.; van den Brom, H. E.; Agrait, N.; van Ruitenbeek, J. M. *Nature* **1998**, *395*, 783–785.
(31) Thijssen, W. H. A.; Marjenburgh, D.; Bremmer, R. H.; van Ruitenbeek, J. M. *Phys. Rev. Lett.* **2006**, *96*, 026806.
(32) Bahn, S. R.; Lopez, N.; Nørskov, J. K.; Jacobsen, K. W. *Phys. Rev. B* **2002**, *66*, 081405.
(33) Untiedt, C.; Yanson, A. I.; Grande, R.; Rubio-Bollinger, G.; Agrait, N.; Vieira, S.; van Ruitenbeek, J. *Phys. Rev. B* **2002**, *66*, 085418.
(34) Rodrigues, V.; Ugarte, D. *Phys. Rev. B* **2001**, *63*, 073405.
(35) Hideaki Ohnishi, Y. K.; Takayanagi, K. *Nature* **1998**, *395*, 780–783.
(36) Skorodumova, N. V.; Simak, S. I. *Phys. Rev. B* **2003**, *67*, 121404.
(37) Legoas, S. B.; Galvão, D. S.; Rodrigues, V.; Ugarte, D. *Phys. Rev. Lett.* **2002**, *88*, 076105.
(38) Olivier, S.; Tréglia, G.; Saúl, A.; Willaime, F. *Surf. Sci.* **2006**, *600*, 5131–5135.
(39) Pyykko, P. *Chem. Rev.* **1988**, *88*, 563–594.
(40) Pyykkö, P. *Angew. Chem.* **2004**, *116*, 4512–4557.
(41) Smit, R. H. M.; Untiedt, C.; Yanson, A. I.; van Ruitenbeek, J. M. *Phys. Rev. Lett.* **2001**, *87*, 266102.
(42) Thijssen, W. H. A.; Strange, M.; aan de Brugh, J. M. J.; van Ruitenbeek, J. M. *New J. Phys.* **2008**, *10*, 033005.
(43) Landmann, M.; Rauls, E.; Schmidt, W. G. *Phys. Rev. B (Condens. Matter Mater. Phys.)* **2009**, *79*, 045412.
(44) Qian, G.-X.; Martin, R. M.; Chadi, D. J. *Phys. Rev. Lett.* **1988**, *60*, 1962–1965.
(45) Esser, N.; Shkrebtii, A. I.; Resch-Esser, U.; Springer, C.; Richter, W.; Schmidt, W. G.; Bechstedt, F.; Del Sole, R. *Phys. Rev. Lett.* **1996**, *77*, 4402–4405.

(46) Reuter, K.; Stampfl, C.; Scheffler, M. Ab initio atomistic thermodynamics and statistical mechanics of surface properties and functions. In Handbook of Materials Modeling, Vol. 1. (Ed.) Sidney Yip. Springer: Berlin Heidelberg, 2005, 149−194.

(47) Rogal, J.; Reuter, K. Ab initio atomistic thermodynamics for surfaces: A primer. In *Experiment, Modeling and Simulation of Gas-Surface Interactions for Reactive Flows in Hypersonic Flights*; Educational Notes RTO-EN-AVT-142; RTO: Neuilly-sur-Seine, 2007.

(48) Kresse, G.; Furthmüller, J. *Comput. Mater. Sci.* **1996**, *6*, 15–50.

(49) Perdew, J. P.; Chevary, J. A.; Vosko, S. H.; Jackson, K. A.; Pederson, M. R.; Singh, D. J.; Fiolhais, C. *Phys. Rev. B* **1992**, *46*, 6671–6687.

(50) Blöchl, P. E. *Phys. Rev. B* **1994**, *50*, 17953–17979.

(51) Kresse, G.; Joubert, D. *Phys. Rev. B* **1999**, *59*, 1758–1775.

(52) Monkhorst, H. J.; Pack, J. D. *Phys. Rev. B* **1976**, *13*, 5188–5192.

(53) Preuss, M.; Schmidt, W. G.; Bechstedt, F. *Phys. Rev. Lett.* **2005**, *94*, 236102.

(54) Blankenburg, S.; Schmidt, W. G. *Phys. Rev. B (Condens. Matter Mater. Phys.)* **2006**, *74*, 155419.

(55) Rauls, E.; Blankenburg, S.; Schmidt, W. *Surf. Sci.* **2008**, *602*, 2170–2174.

(56) Rauls, E.; Schmidt, W. G. *J. Phys. Chem. C* **2008**, *112*, 11490–11494.

(57) Bechstedt, F. *Principles of Surface Physics*; Springer: New York, 2003.

(58) Rauls, E.; Frauenheim, T. *Phys. Rev. B* **2004**, *69*, 155213.

(59) Lange, B.; Schmidt, W. *Surf. Sci.* **2008**, *602*, 1207–1211.

(60) Schwabl, F. *Statistische Mechanik*; Springer: New York, 2006.

(61) Carey, V. P. *Statistical Thermodynamics and Microscale Thermodynamics*; Cambridge University Press: New York, 1999.

(62) Northrup, J. E.; Di Felice, R.; Neugebauer, J. *Phys. Rev. B* **1997**, *56*, R4325−R4328.

(63) Rauls, E.; Hajnal, Z.; Deák, P.; Frauenheim, T. *Phys. Rev. B* **2001**, *64*, 245323.

(64) If the vibrational entropy contributions to the free energy are considered, the clean (1 × 2) reconstruction is stabilized against the clean (1 × 3) surface above 112 K.

(65) *Landolt−Börnstein−Group III Condensed Matter, Volume 24a. Physics of Solid Surfaces−Structure*; Springer: New York, 1993.

(66) Kittel, C. *Einführung in die Festkörpertheorie*; Oldenbourg, 2002.

(67) Huber, K. P.; Herzberg, G. *Molecular Spectra and Molecular Structure, IV Constants of Diatomic Molecules*; Van Nostrand Reinhold: New York, 1997.

(68) Stull, D. R.; Prophet, H. *JANAF Thermochemical Tables*, 2nd ed.; American Institute of Physics: Woodbury, NY, 1971.

(69) Shi, H.; Asahi, R.; Stampfl, C. *Phys. Rev. B (Condens. Matter Mater. Phys.)* **2007**, *75*, 205125.

(70) *Landolt−Börnstein−Group IV Physical Chemistry, Volume 19A, Physics, Landolt−Börnstein, Physical Chemistry and Mechanics, Fluids, Thermodynamics*; Springer: New York, 1999.

(71) As shown in ref 43 coverages in PT1 sites below $\Theta < 0.041 Å^{-2}$ on Au(110)-(1 × 1) and Au(110)-(1 × 2) and $\Theta < 0.0141 Å^{-2}$ on Au(110)-(1 × 3) show characteristics of an isolated atom on the surface.

(72) Légaré, P. *Surf. Sci.* **2005**, *580*, 137–144.

(73) Giannozzi, P.; Car, R.; Scoles, G. *J. Chem. Phys.* **2003**, *118*, 1003–1006.

JP810581S